HHS Public Access

Author manuscript

Science. Author manuscript; available in PMC 2020 December 19.

Published in final edited form as:

Science. 2020 June 19; 368(6497): . doi:10.1126/science.abb2751.

Meissner corpuscles and their spatially intermingled afferents underlie gentle touch perception

Nicole L. Neubarth[1,2,4,*], **Alan J. Emanuel**[1,2,*], **Yin Liu**[3,*], **Mark W. Springel**[1,2], **Annie Handler**[1,2], **Qiyu Zhang**[1,2], **Brendan P. Lehnert**[1,2], **Chong Guo**[1], **Lauren L. Orefice**[1,2], **Amira Abdelaziz**[1,2], **Michelle M. DeLisle**[1,2], **Michael Iskols**[1,2], **Julia Rhyins**[1,2], **Soo J. Kim**[1,2], **Stuart J. Cattel**[1,2], **Wade Regehr**[1], **Christopher D. Harvey**[1], **Jan Drugowitsch**[1], **David D. Ginty**[1,2]

[1]Department of Neurobiology, Harvard Medical School, 220 Longwood Avenue, Boston, MA 02115, USA

[2]Howard Hughes Medical Institute, Harvard Medical School, 220 Longwood Avenue, Boston, MA 02115, USA

[3]Department of Biochemistry, Howard Hughes Medical Institute, Stanford University, 279 Campus Drive, Stanford, CA 94305, USA

[4]Present address: Two Six Labs, 901 North Stuart Street, Arlington, VA 22203, USA

Abstract

Meissner corpuscles are mechanosensory end organs that densely occupy mammalian glabrous skin. We generated mice selectively lacking Meissner corpuscles and found them to be deficient in both perceiving the gentlest detectable forces acting on glabrous skin and fine sensorimotor control. We found that Meissner corpuscles are innervated by two mechanoreceptor subtypes that exhibit distinct responses to tactile stimuli. The anatomical receptive fields of these two mechanoreceptor subtypes homotypically tile glabrous skin in a manner that is offset with respect to one another. Electron microscopic analysis of the two Meissner afferents within the corpuscle supports a model in which the extent of lamellar cell wrappings of mechanoreceptor endings determines their force sensitivity thresholds and kinetic properties.

Corresponding author: david_ginty@hms.harvard.edu.

*equal contributions

Author Contributions

N.L.N., Y.L., A.J.E., and D.D.G. conceived the project; N.L.N and Y.L. performed light microscopy experiments with assistance from A.A.; N.L.N., A.J.E., and B.P.L did *in vivo* electrophysiological recordings with guidance from C.D.H.; M.W.S., M.I., J.R., and S.J.K. performed the operant conditioning behavioral experiments; L.L.O. performed the PPI experiments; N.L.N., A.A., and M.M.D. performed all other behavioral experiments; N.L.N. and J.D. performed the modeling; A.H., Q.Z., and S.J.C. did the EM analysis. N.L.N. and D.D.G. wrote the first draft of the paper, with sections subsequently provided by A.J.E.; All authors contributed to the final manuscript draft.

Competing Interests

The authors have no competing interests.

Data and Materials Availability

All data are available in the manuscript or the supplementary material. Reagents are available from the corresponding author upon reasonable request.

Supplementary Materials

Materials and Methods

Figures S1–S10

Movies S1 and S2

References (30–43)

One Sentence Summary

Glabrous skin light touch perception and fine sensorimotor control arises from spatially overlapping mechanoreceptors of the Meissner corpuscle.

The basic anatomy of the Meissner corpuscle and its presumed innervating Aβ Rapidly Adapting Type I (RA1) low-threshold mechanoreceptor (LTMR) have been widely described since its discovery in 1852 (1). However, the Meissner corpuscle's requirement for touch-related behaviors, sensorimotor capabilities, and tactile perception have remained a matter of speculation.

Mice lacking either brain-derived neurotrophic factor (BDNF) or its receptor TrkB die neonatally and notably also have a complete absence of Meissner corpuscles (2–4). We thus generated conditional mutant mouse models that are viable in adulthood and selectively lack Meissner corpuscles for addressing their role in tactile perception and sensorimotor behaviors in adult animals. We found that BDNF is expressed in glabrous skin during the period of Meissner corpuscle formation (Fig. S1A–C). Eliminating BDNF expression in epithelial cells of the skin using *K5Cre; BDNF*$^{flox/flox}$ mice resulted in a dramatic reduction in the number of Meissner corpuscles (Fig. S1F, G, H). We found no disturbance of Meissner corpuscles in mice lacking BDNF in neurons of the dorsal root ganglia (DRG) or Schwann cells (*Wnt1*^{Cre}*; BDNF*$^{flox/flox}$; Fig. S1D, E, H), suggesting that skin-derived—and not neuron- or Schwann cell-derived—BDNF is crucial for Meissner corpuscle development. BDNF's cognate receptor, TrkB, is present in a subset of primary sensory neurons of the DRG, and mice that selectively lack TrkB in primary sensory neurons (*Advillin*^{Cre}*; TrkB*$^{flox/flox}$, hereafter called *TrkB*^{cKO}) (5, 6), while viable and overtly normal, are also devoid of Meissner corpuscles and their innervating sensory neurons (Fig. 1A, B, Fig. S2). Mice that lack TrkB in Schwann cells, on the other hand, have a normal complement of Meissner corpuscles (Fig. S2H, J). Although some neurofilament-positive (NFH^{+}) sensory fibers were present in glabrous skin dermal papillae of *TrkB*^{cKO} mice prior to P20, these fibers were absent in adults (Fig. 1A, S2). In contrast, Merkel cells and the cutaneous endings of their associated Aβ Slowly Adapting (SA) LTMRs, which are TrkB-negative, were found in comparable numbers in control and *TrkB*^{cKO} adult mice (Fig. 1A, B). We next did *in vivo* loose-patch electrophysiological recordings (7, 8) of random L4 DRG neurons from adult control and *TrkB*^{cKO} mice. While indentation of hindpaw glabrous skin with gentle force steps evoked both Aβ RA-LTMR and Aβ SA-LTMR physiological responses in control mice, Aβ RA-LTMR responses were absent in *TrkB*^{cKO} mice even at indentation forces as high as 75mN (Fig. 1D–F). Activation thresholds and firing patterns of Aβ SA-LTMRs in control and *TrkB*^{cKO} mice were indistinguishable (Fig. 1G). Thus, BDNF and TrkB expressed in glabrous skin epithelial cells and sensory neurons of the DRG, respectively, are essential for development of Meissner corpuscles and the presence of Aβ RA-LTMR responses to indentation of glabrous skin. In contrast, sensory-neuron TrkB signaling is dispensable for the development and normal response properties of Merkel cells and their associated Aβ SA-LTMRs and, as found previously, the development of Pacinian corpuscles (2–4, 9).

We subjected adult control and *TrkB*^{cKO} mice to behavioral tests of glabrous skin sensitivity, light touch perception, gait analysis, and fine sensorimotor control. First, we measured glabrous hindpaw withdrawal thresholds in *TrkB*^{cKO} and littermate control mice using forces ranging from 0.008 g to 4.0 g applied to the pedal pads of the hindpaw (Fig. 2A). Wild-type mice withdrew their paws in response to the entire range of forces presented, rarely reacting to the lowest forces and nearly always reacting to the highest forces. On the contrary, while *TrkB*^{cKO} mice displayed normal hindpaw withdrawal at the high end of this force range, they were unresponsive to the lightest forces (Fig. 2A). We infer from these behavioral measurements that activation of Merkel cell complexes and Aβ SA-LTMRs does not underlie sensorimotor responses to the lightest detectable forces acting on glabrous skin. To further test whether this deficit was specific to disruption of Meissner corpuscles and not to disturbance of Merkel cell complexes, we measured withdrawal thresholds in mice lacking Merkel cells (*K5Cre*; *Atoh1*$^{flox/flox}$ or *Atoh1*^{cKO}) (10–16). In mice lacking Merkel cells, Meissner corpuscles were present in slightly increased numbers (Fig. 1C). Behaviorally, mice lacking Merkel cells performed normally on the von Frey paw withdrawal test (Fig. 2B).

Next, we trained water-deprived mice within an operant conditioning behavioral paradigm to report detection of glabrous skin indentation stimuli by lick retrieval of a water reward (Fig. 2C–E). Mice learned to lick specifically in response to mechanical stimuli within two weeks, at which time we delivered step indentations ranging between 0 and 75 mN to the forepaw and measured perceptual detection thresholds (force at the midpoint of the psychometric function; Fig. 2F). While control mice exhibited perceptual detection thresholds of approximately 10 mN, mice lacking Meissner corpuscles had increased perceptual thresholds of approximately 20 mN. In contrast, reactivity to a light air puff applied to back hairy skin was comparable in control and *TrkB*^{cKO} mice (Fig. S3), indicating normal hairy skin sensitivity.

We next tested the requirement of Meissner corpuscles in an innate, fine sensorimotor behavior: forepaw manipulation of sunflower seeds while eating. The amount of time required to deshell and eat the sunflower seed kernel was comparable for control and *TrkB*^{cKO} mice. However, while control mice used their forepaws to hold, elevate, and rotate the sunflower seed, *TrkB*^{cKO} mice typically trapped or braced the seed on the floor while biting and removing the shell to expose the kernel (Fig. 2; Movies S1 and S2). *TrkB*^{cKO} mice exhibited fewer forepaw dips to the floor and seed rotations and instead more frequently touched the floor to brace the seed. (Fig. 2G). In contrast, gait was largely unaltered in *TrkB*^{cKO} mice, although subtle differences in gait were apparent at high velocities (Fig. S4). We observed no other obvious sensorimotor deficits in *TrkB*^{cKO} mice (Figs. S3 and S4).

Large-diameter, myelinated sensory neurons innervating Meissner corpuscles express the tyrosine kinase Ret beginning on embryonic day 10.5 (E10.5) (9). Consistent with this, *Ret*^{CreER}; *Rosa26*$^{LSL\text{-}tdTomato}$ mice (9, 17) treated with tamoxifen from E10.5 to E13.5 had tdTomato^{+} sensory fibers that innervate Meissner corpuscles (Fig. 3A). Because TrkB^{+} sensory neurons are required for Meissner corpuscle formation, we asked whether these Ret^{+} Meissner afferent fibers also express TrkB. TrkB^{+} axon terminals were present in the dermal

papillae of glabrous skin during embryonic and early postnatal ages, but TrkB expression was undetectable in Meissner afferent terminals in adult mice (Fig. S5). Therefore, to permanently label TrkB$^+$ neurons and visualize their cutaneous endings in glabrous skin of adults, we treated *TrkB^{CreER}*; *Rosa26$^{LSL\text{-}tdTomato}$* mice (18) with tamoxifen between E15.5 and P6. We observed that adult *TrkB^{CreER}*; *Rosa26$^{LSL\text{-}tdTomato}$* mice possess tdTomato$^+$ sensory fibers within Meissner corpuscles (Fig. 3B). These TrkB$^+$ Meissner corpuscle afferents are distinct from Ret$^+$ Meissner corpuscle afferents. Indeed, using *TrkB^{CreER}*; *Rosa26$^{LSL\text{-}tdTomato}$*; *Ret^{CFP}* compound mice (19), the TrkB$^+$ and Ret$^+$ sensory neurons were found to be separate populations, with endings of both of these neuronal populations terminating within the majority of corpuscles in both forepaw and hindpaw glabrous skin (Fig. 3C, E). Dual innervation of corpuscles was also seen using the *Npy2r-GFP* BAC transgenic mouse line, which labels Aβ RA-LTMRs in both hairy and glabrous skin (20). In *TrkB^{CreER}; Rosa26$^{LSL\text{-}tdTomato}$; Npy2r-GFP* compound mice, all GFP$^+$ fibers in the dermal papillae were tdTomato$^+$ (Fig. S5). On the other hand, in *Ret^{CreER}; Rosa26$^{LSL\text{-}tdTomato}$; Npy2r-GFP* compound mice, tdTomato$^+$ and GFP$^+$ fibers in dermal papillae were distinct and intertwined (Fig. 3D). Both the Ret$^+$ and TrkB$^+$ Meissner afferents expressed neurofilament, and together these two neuronal populations accounted for most, if not all, NFH$^+$ Meissner corpuscle endings (Fig. 3C, Fig. S5). Meissner corpuscle lamellar cells, which are specialized terminal Schwann cells, migrated into dermal papillae along Meissner afferent axons during development (Fig. S6), and TrkB$^+$ axons and corpuscle lamellar cells were both absent from dermal papillae of *TrkB^{cKO}* mice. Although axons of Ret$^+$ neurons still projected into dermal papillae in the absence of TrkB$^+$ axons and corpuscle lamellar cells in neonatal *TrkB^{cKO}* mutants, these Ret$^+$ fibers either retracted or degenerated because neither Ret$^+$ nor TrkB$^+$ afferents were present in dermal papillae of adult *TrkB^{cKO}* mice (Fig. S2). Thus, consistent with prior work suggesting multiple, immunohistochemically distinct Meissner corpuscle afferent endings (21), our findings reveal that Meissner corpuscles are co-innervated by a pair of intertwined, molecularly and developmentally distinct populations of sensory neurons, one expressing TrkB and another expressing Ret.

Meissner corpuscles are believed to be innervated by one physiological type of sensory neuron, the Aβ RAI-LTMR (21–24). Our electrophysiological recordings showed that Aβ RA-LTMR responses to glabrous skin stimulation are lost in *TrkB^{cKO}* mice (Fig. 1F). Therefore, we hypothesized that the Ret$^+$ and TrkB$^+$ Meissner afferents are previously unrecognized subsets of Aβ RAI-LTMRs. Aβ RA-LTMRs form central collaterals along the rostrocaudal axis of the spinal cord and also extend an axonal branch via the dorsal column to the dorsal column nuclei (DCN) of the brainstem (25–27). This projection via the direct dorsal column pathway is likely important for tactile perception and discriminative touch (21). We visualized the central projections of both the Ret$^+$ and TrkB$^+$ Meissner afferents. These analyses revealed that both Meissner afferent subtypes display archetypal Aβ LTMR central collateral morphologies and axonal projections to the DCN (Fig. S7).

We next asked whether either or both Ret$^+$ and TrkB$^+$ Meissner afferents have physiological response properties consistent with those of Aβ RAI-LTMRs. We used the *in vivo* DRG recording preparation for targeted electrophysiological recordings of genetically labeled Ret$^+$ and TrkB$^+$ Meissner afferent populations. All recorded Meissner afferents of both subtypes had small, well-defined receptive fields confined to a single glabrous pad. Both subtypes

also had conduction velocities within the Aβ range, although the mean conduction velocity of TrkB$^+$ Meissner afferents was modestly but significantly slower than that of Ret$^+$ Meissner afferents (Fig. 4A). TrkB$^+$ Meissner afferents responded at both the onset and offset of force-controlled step indentations with high sensitivity, whereas Ret$^+$ Meissner afferents responded at the onset of step indentations with lower and more varied sensitivity and rarely responded to the offset of step indentations (Fig. 4B–D). Some (4 of 10) of the Ret$^+$ Meissner afferents responded during the sustained phase of the step indentation (example in Fig. 4E), indicating Meissner-innervating afferents are not always rapidly adapting. Both TrkB$^+$ and Ret$^+$ Meissner afferents exhibited a wide range of frequency tuning to 2–120 Hz sinusoidal vibrations: Some neurons of both types responded best to high frequencies while others had nearly uniform force thresholds across the tested frequencies (Fig. S8). While frequency tuning did not differ between TrkB$^+$ and Ret$^+$ Meissner afferents, TrkB$^+$ Meissner afferents were more sensitive to vibratory stimuli than Ret$^+$ Meissner afferents (Fig. S8). Altogether, while the response properties of TrkB$^+$ Meissner afferents fit the classic Aβ RAI-LTMR definition, those of most Ret$^+$ Meissner afferents do not.

We next investigated the spatial relationships between the cutaneous termination fields of Ret$^+$ and TrkB$^+$ Meissner afferents. Homotypic tiling is a phenomenon in which the anatomical receptive fields of neurons do not spatially overlap with other neurons of their same type. Using whole-mount alkaline phosphatase (AP) staining of sparsely labeled Meissner afferents, we found that the skin innervation areas of individual Ret$^+$ and TrkB$^+$ Meissner afferents are well-demarcated, spatially contiguous, and confined to single glabrous pads (Fig. S9), consistent with the physiological receptive fields being confined to single glabrous pads. Occasionally, two neurons innervating the same toe or pedal pad were labeled (Fig. 5A). In these cases, TrkB$^+$ afferents were never observed to spatially overlap, and only one out of ten pairs of Ret$^+$ afferents occupying the same pad displayed spatial overlap (Fig. 5C). For the single overlapped Ret$^+$ afferent pair, the two arborizations shared only one out of twelve total corpuscles, and this corpuscle was on the border of their termination fields. We also used an intersectional genetic labeling strategy to address homotypic tiling. We generated mice harboring either the $TrkB^{CreER}$ or Ret^{CreER} allele in conjunction with two different Cre-dependent fluorescent reporters, $Rosa26^{LSL\text{-}YFP}$ and $Rosa26^{LSL\text{-}tdTomato}$. We treated these mice with high doses of tamoxifen to randomly and efficiently label individual afferents with one of three possibilities: tdTomato, YFP, or both. Virtually all Meissner corpuscles examined in these mice contained a single-color fiber of a given afferent subtype (Fig. 5B, D) thus confirming homotypic tiling of the two Meissner afferent types. We also compared the peripheral arborizations of sparsely labeled Ret$^+$ and TrkB$^+$ Meissner corpuscle afferents. These two populations exhibited differences in both their surface area size distributions and the number of Meissner corpuscles innervated by individual neurons (Fig. 5E, F; Fig. S9), indicating that the two homotypically tiled Meissner afferent types are heterotypically offset.

One potential advantage of heterotypic overlap of Meissner mechanoreceptors with different force sensitivities is to enable discrimination of a greater range of forces. In this model, spikes emanating from the TrkB$^+$ Meissner Aβ LTMR alone encode the lightest indentation forces whereas spikes from both TrkB$^+$ and Ret$^+$ Meissner mechanoreceptors encode higher

forces. Another potential advantage of heterotypic overlap of homotypically tiled Meissner mechanoreceptors is that population responses to forces that co-activate both Meissner afferent types could enable a heightened ability to detect and localize a point stimulus. We modeled the receptive fields of each of the two Meissner afferent subtypes as homotypically tiled grids that are heterotypically offset and simulated measurements of spatial acuity (Fig. S10). Our simulations indicated that, for a single non-overlapping grid, the number of discriminable spatial locations is equal to the number of neurons (Fig. S10). Simulations using two grids that are homotypically tiled but overlapping and maximally offset with respect to each other revealed that the number of distinct spatial locations doubles for the same number of neurons (Fig. S10). This gain arose from a distributed neural representation that an overlapped arrangement facilitates and may enable an enhanced ability to localize a point stimulus without increasing the number of neurons. Therefore, while functional analyses of mice selectively lacking one or the other Meissner afferent subtype will be needed to test our mathematical modeling findings, we speculate that the heterotypic overlap of homotypically tiled Meissner mechanoreceptor subtypes may enable heightened discriminatory capabilities, at a population level, compared to a simpler arrangement of a single homotypically tiled Meissner afferent type.

The different sensitivities and response kinetics of Ret^+ and $TrkB^+$ Meissner Aβ mechanoreceptors raised the question of whether these mechanoreceptor types form distinct endings within the corpuscle where mechanotransduction occurs. We evaluated the ultrastructural properties of the axonal endings of Ret^+ and $TrkB^+$ Aβ mechanoreceptors within the Meissner corpuscle using electron microscopy. We crossed Ret^{CreER} or $TrkB^{CreER}$ mice to reporter mice that express the peroxidase dAPEX2 targeted to the mitochondrial matrix in a recombinase-dependent manner (28), thereby generating an electron-dense label associated with mitochondria and distributed throughout the labeled cells. We could distinguish and characterize the ultrastructural properties of labeled Aβ mechanoreceptors within the Meissner corpuscle. Axons of both Ret^+ and $TrkB^+$ mechanoreceptor subtypes terminated within the Meissner corpuscle and both ending types were intimately associated with resident, morphologically complex corpuscle lamellar cells (Fig. 6A, B). The lamellar cell processes that surround both Meissner mechanoreceptor ending types were periodically discontinuous, thus exposing the naked mechanoreceptor axonal membrane to the extracellular matrix (Fig. 6C). While Ret^+ Meissner axon profiles were usually surrounded by only a few concentrically arranged lamellar cell processes, the lamellar cell processes associated with $TrkB^+$ Meissner profiles were typically much more elaborate. In fact, $TrkB^+$ Meissner afferents have a minimum of five concentric lamellar processes surrounding the axon terminal (range 5–28), and on average twice as many processes compared to Ret^+ Meissner afferent terminals (range 3–18; Fig. 6C). This ultrastructural difference is particularly noteworthy when considering the distinct response kinetics of Ret^+ and $TrkB^+$ Meissner afferents together with classical studies of the Pacinian corpuscle suggesting that lamellar wrappings are critical for the Pacinian LTMR's response kinetics (29). For the Pacinian afferent, lamellar cell wrappings are believed to be essential for its high selectivity to vibratory stimuli and for producing a generator potential as force is withdrawn during a step offset. Moreover, "unwrapping" or removing Pacinian lamellar cells converted its generator potential from being transient to sustained (29). Our findings that Ret

$^{+}$ Meissner mechanoreceptors are associated with fewer lamellar cell wrappings compared to the TrkB^{+} Meissner LTMR, and that they lack responses at indentation step offsets and occasionally display slowly adapting responses, is consistent with these classical theories.

Our findings show the Meissner corpuscle to be crucial for perception of the gentlest detectable forces acting on the glabrous skin and for fine sensorimotor control during object manipulation. The corpuscle is endowed with intertwined endings of two molecularly, ultrastructurally, and physiologically distinct mechanoreceptor subtypes whose cutaneous innervation areas are homotypically tiled and heterotypically offset. This arrangement of differentially sensitive Meissner Aβ mechanoreceptors supports a "population coding" model for force intensity. Computational simulations suggest that it may enable higher acuity, at a population level, than would be expected from a simpler arrangement with a single Meissner mechanoreceptor subtype. The organization of the Meissner corpuscle afferents' termination fields thus illustrates a solution to the nervous system's general challenge of localizing stimuli with a limited number of neurons. Our EM findings reveal that the axonal endings of the Ret^{+} and TrkB^{+} Meissner Aβ mechanoreceptor subtypes, and in particular their association with concentrically organized processes of corpuscle lamellar cells, are distinct, supporting a model in which ultrastructural properties of mechanoreceptors within a corpuscle dictate their responses.

Supplementary Material

Refer to Web version on PubMed Central for supplementary material.

Acknowledgements

We thank Emily Kuehn for AAV virus characterization, Wei-Chung Lee for providing access to ultramicrotomy equipment, and Robert LaMotte and Jeff Woodbury for assistance with the *in vivo* physiological recording preparation. We thank Michael Rutlin for preliminary analysis of behavioral deficits in *TrkB* conditional mutant mice, Jessica Barowski for help with figures, David Paul for help with electron microscopy quantification, and Tanya Monteiro for technical assistance. We thank Ofer Mazor and Pavel Gorelik of the HMS Research Instrumentation Core Facility for consultation on operant conditioning design and MATLAB code and Josh Huang for discussing unpublished sunflower seed handling measurements. We thank Matthew Pecot, Soha Ashrafi, Nikhil Sharma, and Gordon Fishell for helpful comments on the manuscript.

Funding

N.L.N., M.W.S., Q.Z. and C.G. were Stuart H.Q. & Victoria Quan Fellows at Harvard Medical School. This work was supported by NIH grants NS97344 (D.D.G.), NS105324 (A.J.E.), NS101843 (M.W.S), MH115554 (J.D.), K99 NS101057 (L.L.O.), NS089521 (C.D.H.), NSF GRFP 2014177995 (M.W.S.), a scholar award by the James S. McDonnell Foundation (J.D.), and the Edward R. and Anne G. Lefler Center for Neurodegenerative Disorders (D.D.G.). D.D.G. is an Investigator of the Howard Hughes Medical Institute.

References and Notes

1. Wagner R, Meissner G, Über das Vorhandensein bisher unbekannter eigenthümlicher Tastkörperchen (Corpuscula tactus) in den Gefühlswarzchen der menschlichen Haut and über die Endausbreitung sensitiver Nerven. Nachricten von der Georg-August-Universität und der Königl Gesellschaft der Wissenschaften zu Göttingen 2, 17–30 (1852).
2. González-Martínez T et al., Absence of Meissner corpuscles in the digital pads of mice lacking functional TrkB. Brain Res 1002, 120–128 (2004). [PubMed: 14988041]
3. González-Martínez T et al., BDNF, but not NT-4, is necessary for normal development of Meissner corpuscles. Neurosci Lett 377, 12–15 (2005). [PubMed: 15722178]

4. Perez-Pinera P et al., Characterization of sensory deficits in TrkB knockout mice. Neurosci Lett 433, 43–47 (2008). [PubMed: 18248898]
5. da Silva S et al., Proper formation of whisker barrelettes requires periphery-derived Smad4-dependent TGF-β signaling. Proc Natl Acad Sci U S A 108, 3395–3400 (2011). [PubMed: 21300867]
6. Liu Y et al., Sexually dimorphic BDNF signaling directs sensory innervation of the mammary gland. Science 338, 1357–1360 (2012). [PubMed: 23224557]
7. Bai L et al., Genetic Identification of an Expansive Mechanoreceptor Sensitive to Skin Stroking. Cell 163, 1783–1795 (2015). [PubMed: 26687362]
8. Ma C, Donnelly DF, LaMotte RH, In vivo visualization and functional characterization of primary somatic neurons. J Neurosci Methods 191, 60–65 (2010). [PubMed: 20558205]
9. Luo W, Enomoto H, Rice FL, Milbrandt J, Ginty DD, Molecular identification of rapidly adapting mechanoreceptors and their developmental dependence on Ret signaling. Neuron 64, 841–856 (2009). [PubMed: 20064391]
10. Maricich SM, Morrison KM, Mathes EL, Brewer BM, Rodents rely on Merkel cells for texture discrimination tasks. J Neurosci 32, 3296–3300 (2012). [PubMed: 22399751]
11. Maricich SM et al., Merkel cells are essential for light-touch responses. Science 324, 1580–1582 (2009). [PubMed: 19541997]
12. Morrison KM, Miesegaes GR, Lumpkin EA, Maricich SM, Mammalian Merkel cells are descended from the epidermal lineage. Dev Biol 336, 76–83 (2009). [PubMed: 19782676]
13. Perdigoto CN, Bardot ES, Valdes VJ, Santoriello FJ, Ezhkova E, Embryonic maturation of epidermal Merkel cells is controlled by a redundant transcription factor network. Development 141, 4690–4696 (2014). [PubMed: 25468937]
14. Ramirez A et al., A keratin K5Cre transgenic line appropriate for tissue-specific or generalized Cre-mediated recombination. Genesis 39, 52–57 (2004). [PubMed: 15124227]
15. Shroyer NF et al., Intestine-specific ablation of mouse atonal homolog 1 (Math1) reveals a role in cellular homeostasis. Gastroenterology 132, 2478–2488 (2007). [PubMed: 17570220]
16. Van Keymeulen A et al., Epidermal progenitors give rise to Merkel cells during embryonic development and adult homeostasis. J Cell Biol 187, 91–100 (2009). [PubMed: 19786578]
17. Madisen L et al., A robust and high-throughput Cre reporting and characterization system for the whole mouse brain. Nat Neurosci 13, 133–140 (2010). [PubMed: 20023653]
18. Rutlin M et al., The cellular and molecular basis of direction selectivity of Aδ-LTMRs. Cell 159, 1640–1651 (2014). [PubMed: 25525881]
19. Uesaka T, Nagashimada M, Yonemura S, Enomoto H, Diminished Ret expression compromises neuronal survival in the colon and causes intestinal aganglionosis in mice. J Clin Invest 118, 1890–1898 (2008). [PubMed: 18414682]
20. Li L et al., The functional organization of cutaneous low-threshold mechanosensory neurons. Cell 147, 1615–1627 (2011). [PubMed: 22196735]
21. Abraira VE, Ginty DD, The sensory neurons of touch. Neuron 79, 618–639 (2013). [PubMed: 23972592]
22. Iggo A, Ogawa H, Correlative physiological and morphological studies of rapidly adapting mechanoreceptors in cat's glabrous skin. J Physiol 266, 275–296 (1977). [PubMed: 853451]
23. Willis WD, Coggeshall RE, Sensory mechanisms of the spinal cord. (Kluwer Academic/Plenum Publishers, New York, ed. 3rd, 2004), vol. 1.
24. Johnson KO, The roles and functions of cutaneous mechanoreceptors. Curr Opin Neurobiol 11, 455–461 (2001). [PubMed: 11502392]
25. Brown AG, Fyffe RE, Noble R, Projections from Pacinian corpuscles and rapidly adapting mechanoreceptors of glabrous skin to the cat's spinal cord. J Physiol 307, 385–400 (1980). [PubMed: 7205669]
26. Pubols LM, Pubols BH Jr., Modality composition and functional characteristics of dorsal column mechanoreceptive afferent fibers innervating the raccoon's forepaw. J Neurophysiol 36, 1023–1037 (1973). [PubMed: 4761717]

27. Shortland P, Woolf CJ, Morphology and somatotopy of the central arborizations of rapidly adapting glabrous skin afferents in the rat lumbar spinal cord. J Comp Neurol 329, 491–511 (1993). [PubMed: 8454737]
28. Zhang Q, Lee WA, Paul DL, Ginty DD, Multiplexed peroxidase-based electron microscopy labeling enables simultaneous visualization of multiple cell types. Nat Neurosci 22, 828–839 (2019). [PubMed: 30886406]
29. Loewenstein WR, Mendelson M, Components of receptor adaptation in a Pacinian corpuscle. J Physiol 177, 377–397 (1965). [PubMed: 14321486]
30. Hooks BM, Lin JY, Guo C, Svoboda K, Dual-channel circuit mapping reveals sensorimotor convergence in the primary motor cortex. J Neurosci 35, 4418–4426 (2015). [PubMed: 25762684]
31. Badea TC et al., New mouse lines for the analysis of neuronal morphology using CreER(T)/loxP-directed sparse labeling. PLoS One 4, e7859 (2009). [PubMed: 19924248]
32. Madisen L et al., Transgenic mice for intersectional targeting of neural sensors and effectors with high specificity and performance. Neuron 85, 942–958 (2015). [PubMed: 25741722]
33. Wu H, Williams J, Nathans J, Morphologic diversity of cutaneous sensory afferents revealed by genetically directed sparse labeling. Elife 1, e00181 (2012). [PubMed: 23256042]
34. Gorski JA, Zeiler SR, Tamowski S, Jones KR, Brain-derived neurotrophic factor is required for the maintenance of cortical dendrites. J Neurosci 23, 6856–6865 (2003). [PubMed: 12890780]
35. Danielian PS, Muccino D, Rowitch DH, Michael SK, McMahon AP, Modification of gene activity in mouse embryos in utero by a tamoxifen-inducible form of Cre recombinase. Curr Biol 8, 1323–1326 (1998). [PubMed: 9843687]
36. Jaegle M et al., The POU proteins Brn-2 and Oct-6 share important functions in Schwann cell development. Genes Dev 17, 1380–1391 (2003). [PubMed: 12782656]
37. Badea TC, Cahill H, Ecker J, Hattar S, Nathans J, Distinct roles of transcription factors brn3a and brn3b in controlling the development, morphology, and function of retinal ganglion cells. Neuron 61, 852–864 (2009). [PubMed: 19323995]
38. Gong S et al., A gene expression atlas of the central nervous system based on bacterial artificial chromosomes. Nature 425, 917–925 (2003). [PubMed: 14586460]
39. Guo ZV et al., Flow of cortical activity underlying a tactile decision in mice. Neuron 81, 179–194 (2014). [PubMed: 24361077]
40. Orefice LL et al., Peripheral Mechanosensory Neuron Dysfunction Underlies Tactile and Behavioral Deficits in Mouse Models of ASDs. Cell 166, 299–313 (2016). [PubMed: 27293187]
41. Machado AS, Darmohray DM, Fayad J, Marques HG, Carey MR, A quantitative framework for whole-body coordination reveals specific deficits in freely walking ataxic mice. Elife 4, (2015).
42. Newell A, Yang K, Deng J, Stacked Hourglass Networks for Human Pose Estimation. arXiv e-prints. 2016.
43. Cardona A et al., TrakEM2 software for neural circuit reconstruction. PLoS One 7, e38011 (2012). [PubMed: 22723842]

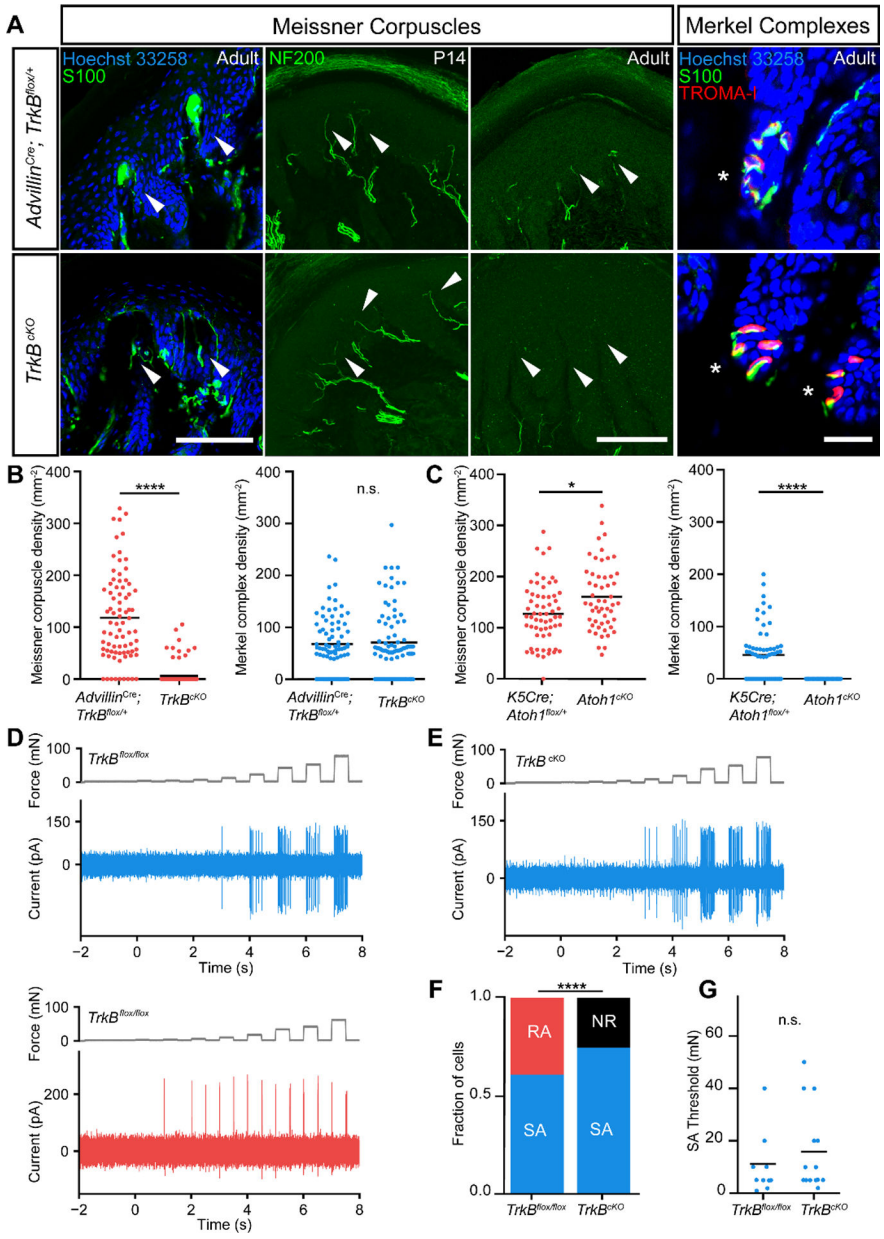

Fig. 1. Meissner corpuscles and their innervating Aβ-LTMRs are absent in *TrkB*^{cKO} mice.

A. Digital pad sections from control (upper panels) and *TrkB*^{cKO} mice (lower panels). Arrows and asterisks indicate typical locations of Meissner corpuscles and Merkel complexes, respectively. Meissner corpuscles and their afferents are labeled with S100 or NFH immunostaining in separate sections, respectively (scale bar = 100 μm). Merkel cells and associated nerve terminals are labeled with TROMA-I and S100, respectively (scale bar = 25 μm). B. Meissner corpuscle and Merkel complex density in glabrous pads of control and *TrkB*^{cKO} mice. Dots represent individual sections, and black bars represent mean. (79 sections from 3 control mice and 81 sections from 3 *TrkB*^{cKO} mice; two-tailed Mann-Whitney test, **** $p < 0.0001$ ($U = 580$), n.s. = not significant ($U = 3163$, $p = 0.9016$)). C. Meissner corpuscle and Merkel complex density in pads of *K5Cre; Atoh1*$^{flox/+}$ and

Atoh1^{cKO} (*K5Cre; Atoh1*$^{flox/flox}$) mice. Dots represent densities from individual sections and black bars represent means. (62 sections from 2 *K5Cre; Atoh1*$^{flox/+}$ animals and 53 sections from 2 *Atoh1*^{cKO} animals; two-tailed Mann-Whitney test, * $p = 0.0113$ ($U = 1193$), **** $p < 0.0001$ ($U = 689$)). D. *In vivo* recordings of a slowly adapting (SA, top, blue) and a rapidly adapting (RA, bottom, red) Aβ-LTMR from control mice in response to step indentations applied to glabrous hindpaw pedal pads (force records shown in gray). E. Example recording of an Aβ SA-LTMR from a *TrkB*^{cKO} mouse in response to the same stimulus as in D. F. Proportion of neurons that are SA, RA, and not responsive (NR) to indentation in control (left, n = 18 cells) and *TrkB*^{cKO} mice (right, n = 20 cells). χ^2 test: $\chi^2 = 8.5$, $p = 0.004$. G. Mean (black bars) and individual (circles) thresholds of Aβ SA-LTMRs in control (left, n = 11 cells) and *TrkB*^{cKO} mice (right, n = 15 cells). Unpaired t-test: $t = -0.81$, $p = 0.42$.

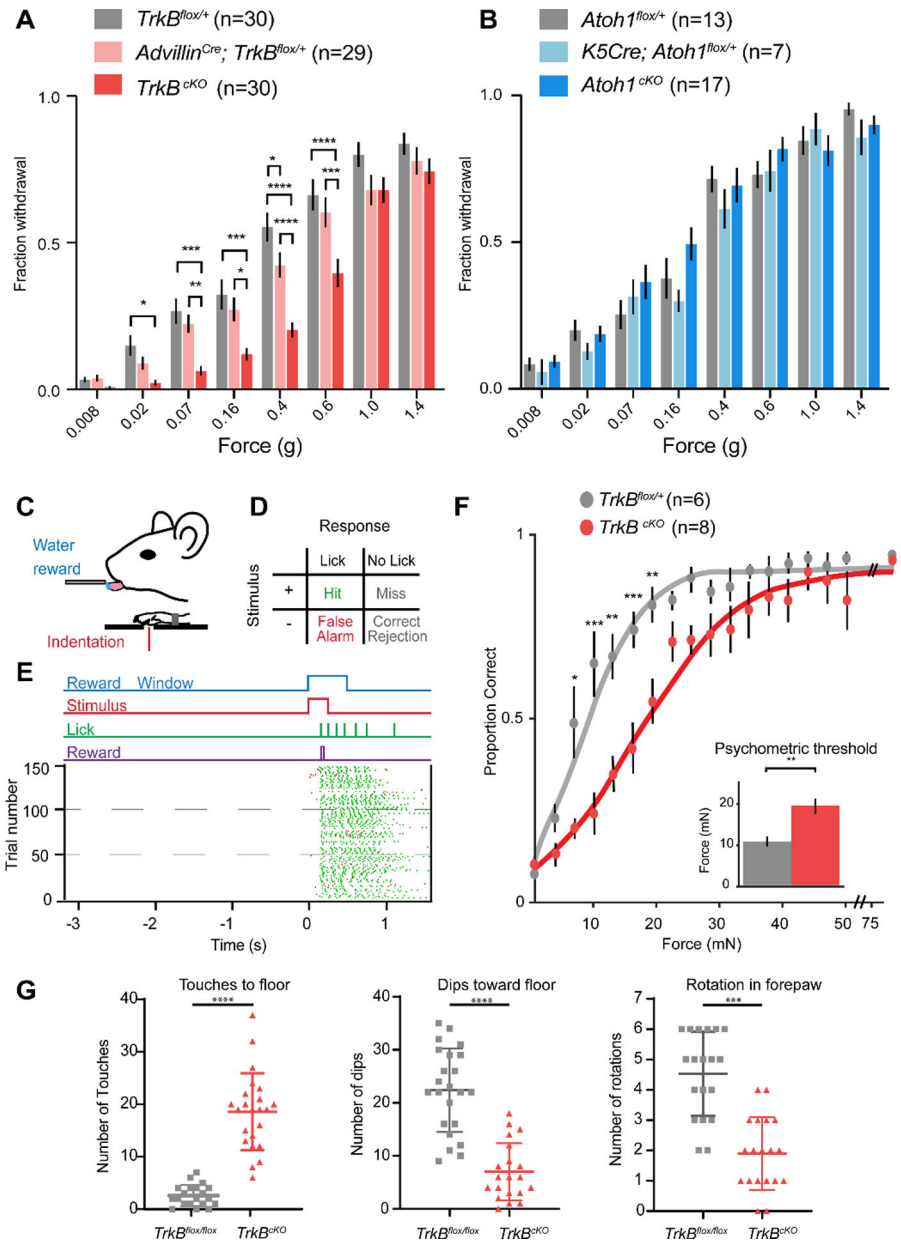

Fig. 2. Meissner corpuscles are necessary for light touch perception and fine sensorimotor control.

A. Fraction (mean ± s.e.m.) of paw withdrawals to von Frey filament applications for *TrkB*^{cKO} and control mice. RM two-way ANOVA, effect of genotype ($F_{(2,86)} = 9.823$, $p = 0.0001$) with post-hoc Tukey's; p-values represent comparisons between genotypes for each filament: * $p < .05$, ** $p < .01$, *** $p < .001$, **** $p < .0001$ B. Same as A for *Atoh1*^{cKO} and control mice. RM two-way ANOVA, no effect of genotype: $F_{(2,34)} = 0.8258$, $p = 0.4465$ C. Operant conditioning task design. D. Matrix of possible behavioral outcomes from one trial. E. Operant conditioning task. (Top) Stimulus paradigm, where animals must withhold for at least 3 seconds before initiation of a new trial. On trials with a stimulus (shown), animal receive rewards only on hit trials. (Bottom) Raster plot of licks. Hit trials shown with green ticks, False alarm trials shown with red ticks. F. Psychometric functions for the operant

conditioning task for *TrkB*^{cKO} and control mice. Error bars represent s.e.m. (Inset shows thresholds; unpaired t-test: t = 2.69, p = 0.002). Two-way ANOVA, effect of genotype ($F_{(1,12)} = 8.261$, p = 0.0140) with post-hoc Sidak's multiple comparison; p-values represent comparisons between genotypes for each force range: * p < 0.05, ** p < 0.01, *** p < 0.001, **** p < 0.0001. G. Left, the number of sunflower seed touch-taps when the seed is braced against the floor between forepaws during seed peeling. Middle, the number of times the mouse held the seed in an elevated position and used its incisors to bite into the seed while applying downward force (dips) to expose seed kernel. Right, the number of seed rotations as mice adjusted their grasp. Unpaired student's test, *** p < 0.001 **** p < 0.0001.

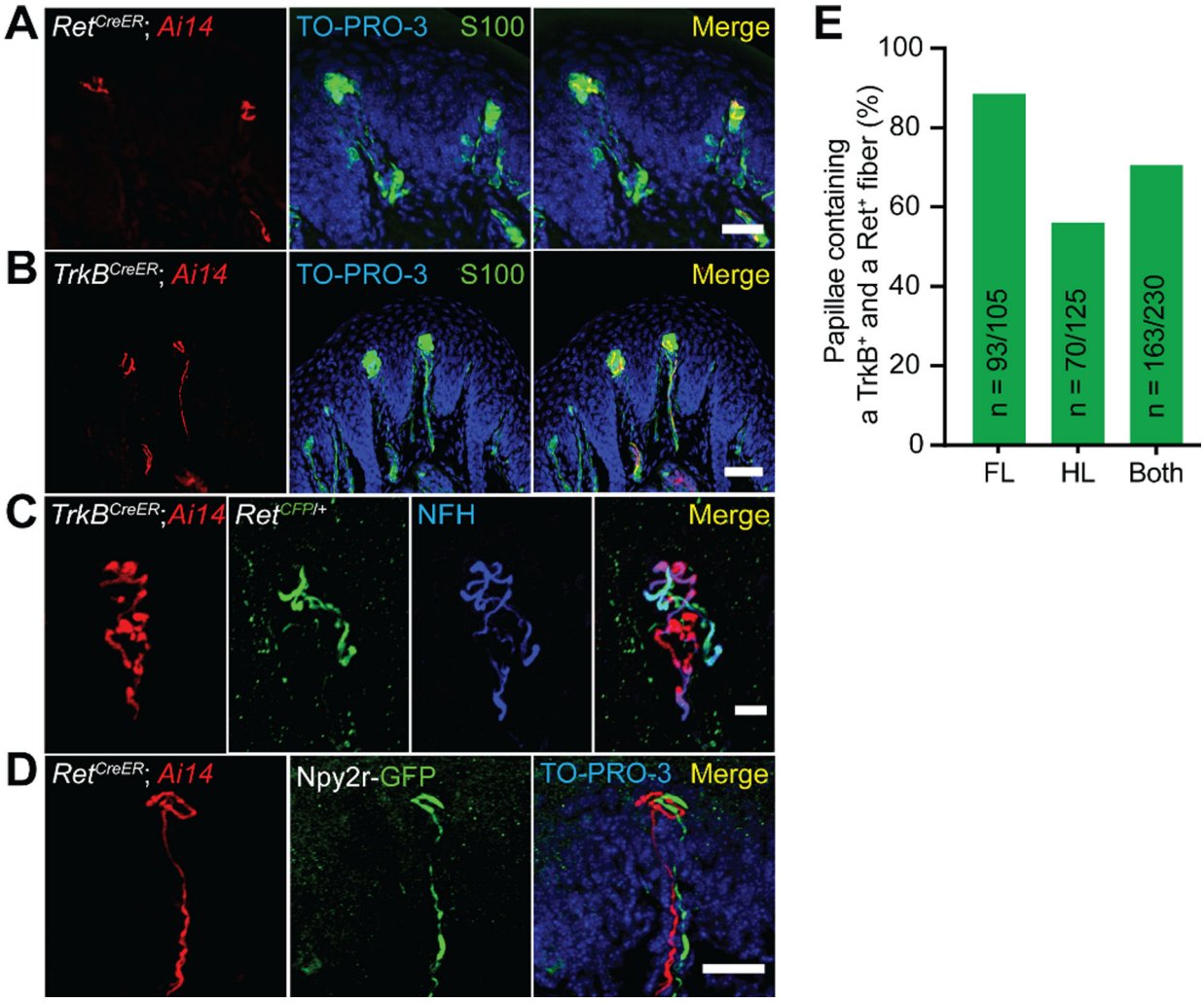

Fig. 3. Meissner corpuscles are innervated by two molecularly distinct mechanosensory neuron types.

A. Forelimb pedal pad section of a P20 *Ret*^{CreER}*; Rosa26*$^{LSL\text{-}tdTomato}$ (*Ai14*) mouse treated with tamoxifen at E10.5-E11.5. Section is immunostained for S100, DsRed, and TO-PRO-3. This experiment was repeated in 3 mice. Scale bar = 25 μm B. Hindlimb digital pad section of a P50 *TrkB*^{CreER}*; Rosa26*$^{LSL\text{-}tdTomato}$ (*Ai14*) mouse treated with tamoxifen at E16.5. Section is stained for S100, DsRed, and TO-PRO-3. This experiment was performed in 8 mice with varying dates of tamoxifen administration (E13.5, E16.5, P2, and P6). Scale bar = 50 μm. C. Hindlimb digital pad section of a P50 *TrkB*^{CreER}*; Ai14; Ret*^{CFP} mouse treated with tamoxifen at P5. Section is immunostained for DsRed, GFP, and NFH. This experiment was repeated in 4 mice with tamoxifen administration at E13.5 or P5. This experiment was repeated in 3 mice. Scale bar = 10 μm. D. Forelimb pedal pad section of a P20 *Ret*^{CreER}*; Ai14; Npy2r-GFP* mouse treated with tamoxifen at E10.5. Section is stained with anti-DsRed, anti-GFP, and TO-PRO-3. Scale bar = 25 μm. E. Percentage of dermal papillae containing both TrkB^{+} and Ret^{+} Meissner afferents in forelimb pads, hindlimb pads, and all pads as measured in *TrkB*^{CreER}*; Ai14; Ret*^{CFP} mice (2 animals). Only papillae containing a

tdTomato^{+} fiber were included in the quantification to eliminate an effect of Cre-lox efficiency on the interpretation of these measurements.

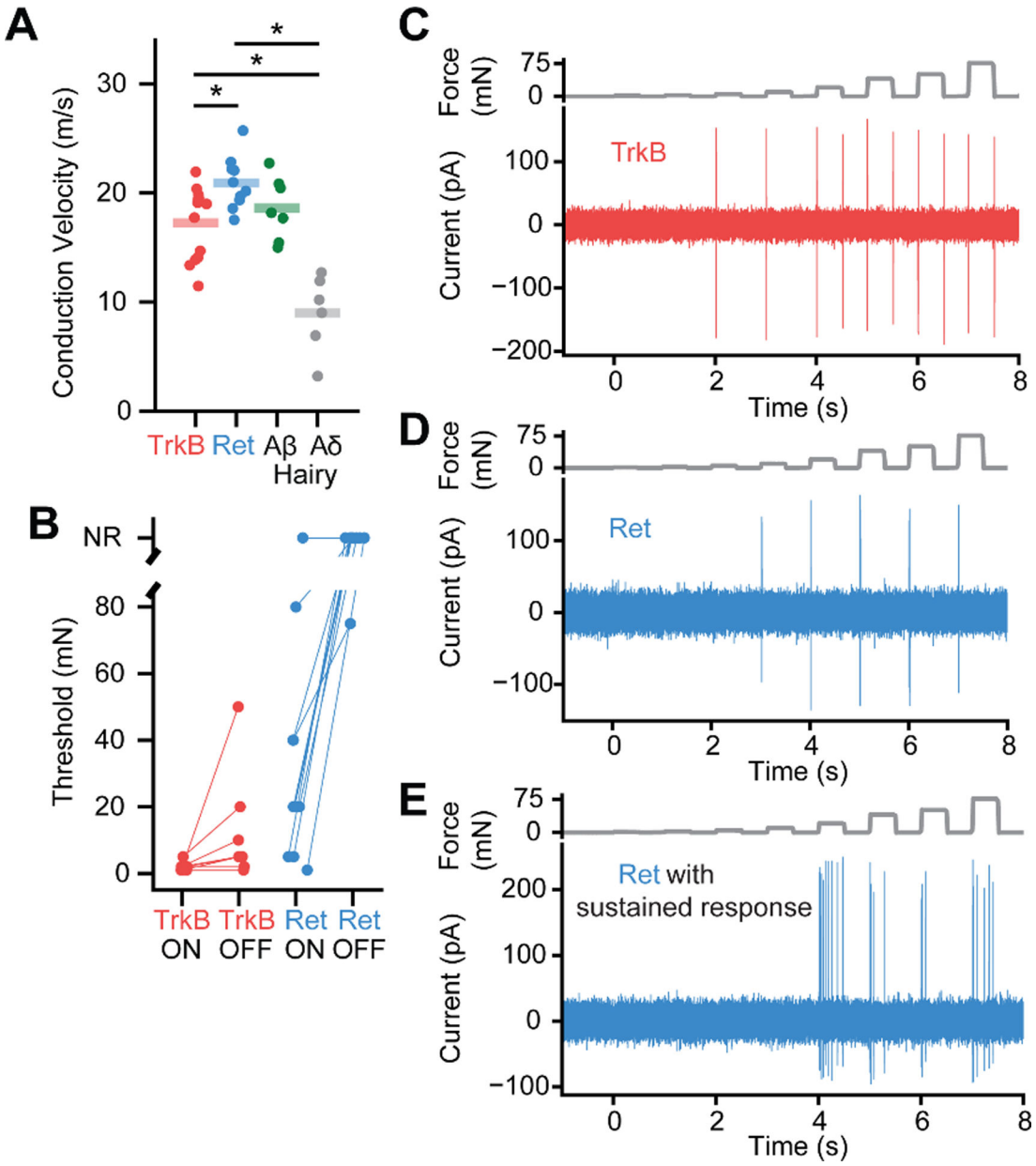

Fig. 4. Ret$^+$ and TrkB$^+$ Meissner afferents exhibit distinct physiological response properties.

A. Both Meissner afferent subtypes have conduction velocities in the Aβ range as defined by the range of conduction velocities measured from hairy skin Aδ and Aβ LTMRs in the same preparation. The average conduction velocities for TrkB$^+$ and Ret$^+$ Meissner afferents are significantly different (10 afferents per type; mean ± s.e.m.: TrkB = 17.3 ± 0.9 m/s, Ret = 20.9 ± 0.8; Mann-Whitney U Test (U = 26.0, p = 0.008). * p < 0.05. B. The minimal force required to produce an action potential at the onset or offset of a step indentation for TrkB$^+$ and Ret$^+$ Meissner afferents. C. Response of a TrkB$^+$ Meissner Aβ LTMR to a series of step indentations increasing in intensity from 1 to 75 mN. D. Response of a RA Ret$^+$ Meissner afferent to the same stimuli as in C. E. Response of a SA Ret$^+$ Meissner afferent.

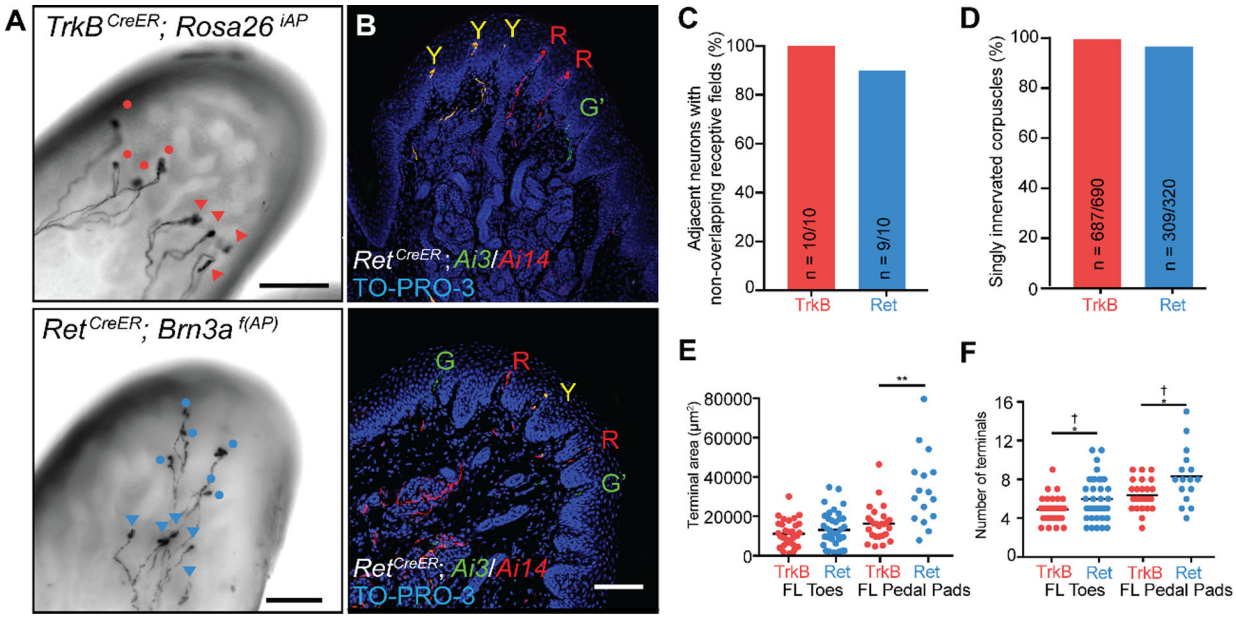

Fig. 5. Spatial arrangement of Ret$^+$ and TrkB$^+$ Meissner afferent cutaneous endings.

A. Images of whole-mount, AP-stained digital pads of a *TrkB^{CreER}; Rosa26^{iAP}* mouse (top) and a *Ret^{CreER}; Brn3a$^{f(AP)}$* mouse (bottom, Z-projection performed in Fiji) depicting pairs of afferents of the same subtype innervating the same glabrous pad. Tamoxifen doses were titrated to achieve sparse labeling of Meissner afferents. Terminals of one neuron are annotated with circles and terminals of the other with triangles. (scale bars = 100 µm) B. Digital pad sections of *TrkB^{CreER}; Rosa26$^{LSL\text{-}YFP/LSL\text{-}tdTomato}$* (*Ai3/Ai14*) mice treated with tamoxifen at E12.5 and E13.5 (upper panel) and *Ret^{CreER}; Ai3/Ai14* mice administered tamoxifen at E11.5 and E12.5 (lower panel). Y: fibers express both tdTomato and YFP; R: fibers express tdTomato only; G: fibers express YFP only; G': YFP$^+$ fibers without terminals in the sections. Sections were stained with anti-DsRed, anti-GFP, and TO-PRO-3. (scale bar = 100 µm) C. Percentage of TrkB$^+$ and Ret$^+$ Meissner afferent pairs innervating the same pad and occupying different spatial territories. D. Quantification of the percentage of dermal papillae and Meissner corpuscles receiving a single TrkB$^+$ fiber (3 animals) and a single Ret$^+$ fiber (6 animals).

E. Receptive field surface area (terminal area, left) and number of terminal endings (right) of TrkB$^+$ and Ret$^+$ Meissner afferents measured in *TrkB^{CreER}; Rosa26^{iAP}* or *TrkB^{CreER}; Brn3a$^{f(AP)}$* mice (N = 21) and *Ret^{CreER}; Rosa26^{iAP}* or *Ret^{CreER}; Brn3a$^{f(AP)}$* mice (N = 21). Individual measurements and mean values (black bar) are plotted for forelimb digital pads and pedal pads. (two-tailed Welch's t-test, mean significantly different: * $p < .05$, ** $p < .01$; F-test of the equality of variances, variance significantly different: † $p < .01$).

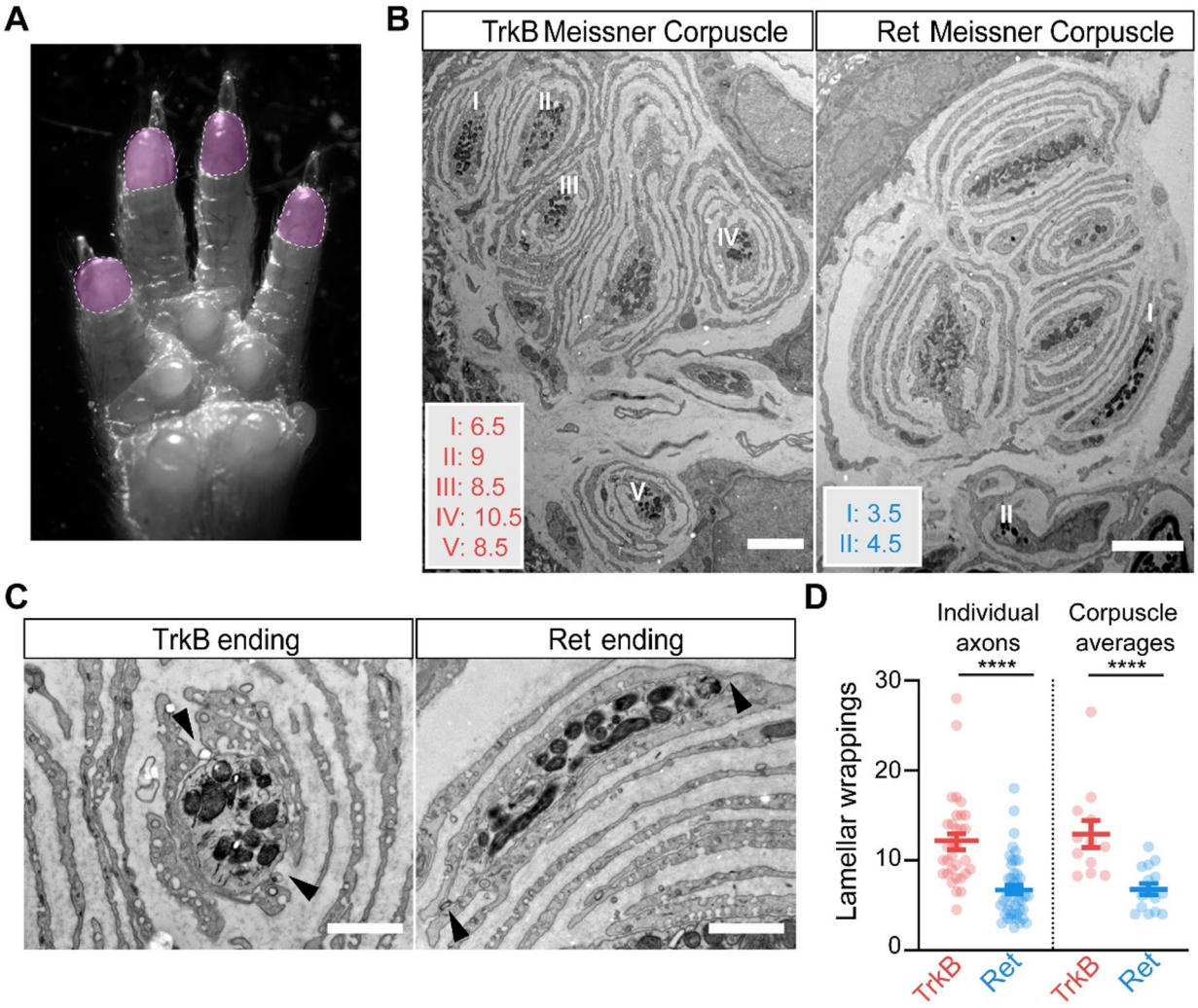

Fig. 6. TrkB^{+} Meissner Aβ LTMR endings have more lamellar cell wrappings than Ret^{+} Meissner mechanoreceptor endings.

A. Image of the paw, with the shaded areas (digit tips) representing regions of high density of Meissner corpuscles used for EM analysis. B. EM images of Meissner corpuscles from a *TrkB^{CreER}; Advillin^{FlpO}; Rosa26$^{DR\text{-}Matrix\text{-}dAPEX2}$* mouse treated with tamoxifen at P3 (left) and a *Ret^{CreER}; Advillin^{FlpO}; Rosa26$^{DR\text{-}Matrix\text{-}dAPEX2}$* mouse treated with tamoxifen at E11.5 and P10 (right). Scale bar = 3 μm. C. High magnification images of labeled endings and associated lamellar cells from (B). Both exhibit openings or areas not directly associated with lamellar cells (black arrowheads). Scale bar = 1 μm. D. Quantification of the number of lamellar cell wrappings around genetically labeled endings of TrkB and Ret endings. Shown are the number of lamellar wrappings for individual axonal profiles (left panel; n = 32 and 47, respectively) and averages of all axonal profiles within individual corpuscles (right panel; n = 12 and 15, respectively). Mann-Whitney *U* test, **** $p < 0.0001$. N = 2 animals for each LTMR subtype.